Composites: Part A 48 (2013) 144–152

Contents lists available at SciVerse ScienceDirect

Composites: Part A

journal homepage: www.elsevier.com/locate/compositesa

Plastic shear bands and fracture toughness improvements of nanoparticle filled polymers: A multiscale analytical model

Marco Salviato, Michele Zappalorto, Marino Quaresimin *

University of Padova, Department of Management and Engineering, Stradella S. Nicola 3, 36100 Vicenza, Italy

ARTICLE INFO

Article history:
Received 16 August 2012
Received in revised form 16 January 2013
Accepted 19 January 2013
Available online 29 January 2013

Keywords:
A. Nano-structures
B. Interface/Interphase
B. Fracture toughness
Shear bands

ABSTRACT

In this paper a multiscale model is provided to assess the toughening improvements in nanoparticle filled polymers caused by the formation of localised plastic shear bands, initiated by the stress concentrations around nanoparticles. The model quantifies the energy absorbed at the nanoscale and accounts for the emergence of an interphase zone around the nanoparticles. It is proved that the elastic properties of the interphase, which are different from those of the matrix, due to chemical interactions, highly affect the stress field rising around particles and the energy dissipation at the nanoscale.

1. Introduction

Throughout the last decades the subject of improving the mechanical properties of polymers by the addition of particle fillers has received a large attention. However, only recently nanotechnology has emerged providing very promising results in increasing the mechanical properties of polymers by the addition of nanosized fillers. This is the reason why nanocomposites have received a higher and higher interest by the scientific community, especially for the significant amelioration in terms of stiffness, strength and toughness which can be obtained at low nanofiller contents (see amongst others, [1,2]). It is acknowledged that the reasons for such improvements must be sough in the huge amount of energy dissipated by the numerous damaging mechanisms taking place at the nanoscale. This is the reason why, it is suggested that the best approach to address the prediction of nanocomposite toughness should be a "multi-mechanism" modelling strategy, in which each contribution is weighted according to the specific case (accounting for the type, the morphology and the functionalisation of the nanofiller as well as the loading conditions) [3–7].

However, the modelling of nanoscale damage mechanisms is far from easy and requires a different way of thinking with respect to the approaches developed for traditional composites where two different characteristic lengths at most (microscale and macroscale) are reasonably described by means of continuum mechanics.

When dealing with nanocomposites, the handshaking of nanoscale, microscale and macroscale quantities and phenomena urges a multiscale modelling strategy [6]. Indeed, the introduction of atomistic models, able to account for molecular interactions between nanofillers and the matrix, up to macro length-scales is limited by the impracticability of accounting for more than some hundred millions of atoms. Initial steps towards modelling strategies which account for nanostructure features, such as nano-reinforcement size and distributions, are due to Chen et al. [8]. They provided a simple size-dependent formulation for the debonding stress, later used to compute the energy dissipation due to this mechanism. The analysis carried out in [8] has been later extended by Zappalorto et al. [9] who developed a closed form expression for the critical debonding stress accounting for the existence of an interphase zone embedding the nanoparticle. Such a zone is thought of as characterised by chemical and physical properties different from those of the nanoparticle and of the matrix. On parallel tracks, the effects of surface elastic constants on the debonding stress of nanoparticles have been investigated by Salviato et al. [10] who showed that the range of the nanoparticle radii where those effects are significant is limited to the nanoscale.

Independently, Lauke [7] and Williams [11] analysed the energy dissipation phenomena by considering, besides particle debonding, voiding and subsequent yielding of the polymer. While analysing the fracture toughness improvements resulting from nanomodification of epoxy resins with silica nanoparticles, Hsieh et al. [4,5] experimentally observed two dominant mechanisms responsible of toughening improvements: localised shear banding of the polymer and particle debonding followed by subsequent plastic void growth. They also modified a previous model due to Huang and Kinloch [12] with the aim to assess the fracture toughness improvements resulting from nanomodification. Such a solution,

* Corresponding author. Tel.: +39 0444 998723; fax: +39 0444 998888.
E-mail address: marino.quaresimin@unipd.it (M. Quaresimin).

1359-835X/$ - see front matter © 2013 Elsevier Ltd. All rights reserved.
http://dx.doi.org/10.1016/j.compositesa.2013.01.006

which was proved to be in a very good agreement with the experimental data, requires some quantities to be set on the basis of fracture surface observations. The present authors have recently developed a hierarchical multi-scale model to assess the fracture toughness improvements due to the debonding of nanoparticles and the plastic yielding of nanovoids [13–15]. In more details, it has been shown that the energy absorbed through nanoparticle debonding is almost negligible, but debonding is a necessary condition for the subsequent plastic yielding around nanovoids created by debonded nanoparticles, such a toughening mechanism being, instead, of primary concern. The model quantifies the energy absorbed at the nanoscale and accounts for the emergence of an interphase zone around the nanoparticles [13–15]. The experimental observations carried out in [4,5] allow to state that different damaging mechanisms, taking place at the nanoscale, can simultaneously contribute to the overall fracture toughness of the nanocomposite. Accordingly, the nanocomposite toughness can be written as $G_{Ic} = G_{Im} + \sum_i \Delta G_i$, where G_{Im} is the toughness of the unloaded matrix and ΔG_i is the toughness improvement due to the i-th damaging mechanism. Then, the best approach to predict the nanocomposite toughness should be a "multi-mechanism" modelling strategy, in which each ΔG_i contribution is appropriately determined and weighted according to the specific case [6]. As a further step towards this multimechanism strategy, in the present paper we address the multiscale modelling of the toughness improvement due to shear banding around nanoparticles. The major novelty of the present paper, with respect to those above mentioned dealing with the same topic [4,5], lays on the fact that the effect of an interphase zone surrounding the nanoparticle, characterised by mechanical properties different from those of the constituents, is explicitly considered. Zappalorto et al. [9] have already demonstrated that the interphase properties (which are linked to surface functionalizers) have a significant effect on the debonding stress, especially for nanoparticle radii below 50 nm.

Briefly, the aims of the present paper can be summarised as follows:

- to quantify the toughness improvement due to the shear banding around nanoparticles. Shear bands are supposed to be initiated by the stress concentrations around the periphery of the nanoparticles;
- to show that the formation of local shear bands is a highly dissipative mechanism, causing a high fracture toughness improvement at low nanofiller content;
- to prove that nanocomposite toughening may be strongly affected by the size of nanoparticles and by surface treatments. In particular, the effect of functionalisation is accounted for through the properties and the size of the interphase.

It is worth mentioning here again that the correct estimation of the fracture toughness improvement resulting from nanomodification requires the modelling of all the possible damage mechanisms taking place at the nanoscale. Accordingly this work has to be seen as a part of a more general multiscale model including the contributions of other mechanisms analysed in previous works [13–15].

2. Description of the hierarchical multiscale strategy adopted for the analysis

2.1. General concepts

Modelling of nanocomposite mechanical properties urges to deal with three different length scales, macro-, micro- and nano-, each of them being characterised by peculiar phenomena and mechanical quantities. Accordingly, we will use terms like "macroscale stress" or "microscale stress" and, in order to avoid misunderstandings it is worth giving the correct definitions for these quantities and briefly discussing the link between them.

Macro-scale: at the macroscale, the material is assumed to be homogeneously and continuously distributed "so that the smallest element cut from the body possesses the same specific physical properties as the body" [16]. In addition, under the hypothesis that the nanofiller is randomly oriented and uniformly distributed, the material can also be thought of as isotropic. All the mechanical quantities (such as stresses and strains) are regarded as averaged values [17] and supposed to be representative of the overall material behaviour.

Micro-scale: the micro-scale system is commonly described as a RVE (Representative Volume Element) and it has to be large enough to be statistically representative of the properties of the material system. Contemporaneously, whenever the nanofiller is uniformly distributed and dispersed, the microscale system can be regarded to be, within reason, sufficiently small to be an infinitesimal volume of the macro-scale one. All the microscale mechanical properties are considered here as pointwise values [17].

Nano-scale: the nanoscale system represents a single unit cell of those compounding the micro-scale system; it accounts for the material morphology (such as nanofiller type and size).

Macroscale stresses, σ, can be regarded as the average values over a RVE of the microscale stresses [17–19]:

$$\sigma = \frac{1}{V}\int_V \hat{\sigma} dV \tag{1a}$$

where $\hat{\sigma}$ is the micro-scale stress distributions and V is the volume of the RVE.

The handshaking between the mechanical quantities characterising the different length scales can be carried out thanks to the Mori–Tanaka theorem, which allows to disregard of the actual microscale fields by approximating stresses on the boundary of nano-inhomogeneities (nanoscale). If the considered volume fractions are small enough to avoid significant particle–particle interactions, this can be carried out taking advantage of the Global Concentration Tensors of Eshelby dilute solution, **H**, and of the mean value for the fields over the RVE which, thanks to Eq. (1a) equate the macroscale ones:

$$\sigma_n = \mathbf{H} : \left\{\frac{1}{V}\int_V \hat{\sigma} dV\right\} = \mathbf{H} : \sigma \tag{1b}$$

The procedure just described is also summarised in the flow chart shown in Fig. 1.

2.2. Multiscale strategy to analyse shear bands around nanoparticles

2.2.1. Description of the nanoscale system

Different from traditional microsized composites, in nanoscale materials and structures the surface effects become important [20–22] due to the high surface/volume ratio.

The significant effect of the elastic properties of the interphase on the critical debonding stress around nanoparticles has been recently shown by Zappalorto et al. [9]. This solution proves that, since different functionalizers lead to different elastic properties of the interphase, the debonding stress is highly affected by the surface treatment depending on the interphase radius to the nanoparticle radius ratio, $\mathbf{a}/r_0$.

Unfortunately, the lack of precise data about the law of variation of the interphase properties across its thickness [23] urges to assume, according to [9,24,25] that a through-the-thickness

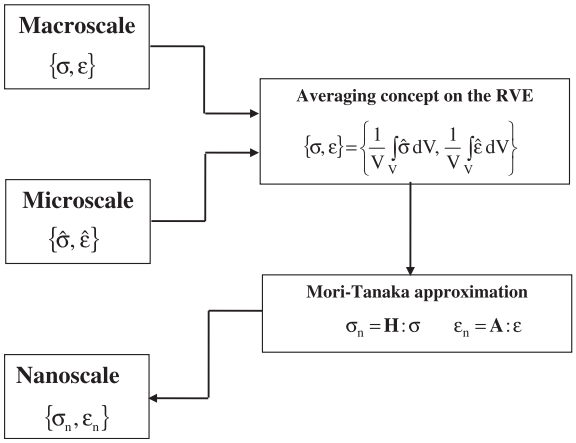

Fig. 1. Flowchart of the multiscale approach adopted in the present work.

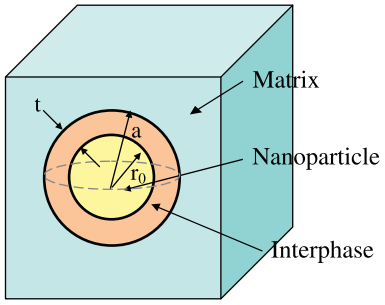

Fig. 2. Description of the system under analysis at the nanoscale.

average is representative of the overall property distribution within the interphase. Consequently, the interphase is supposed to be homogeneous and isotropic.

The system under investigation at the nanoscale, shown in Fig. 2, is constituted by:

- a spherical nanoparticle of radius $\boldsymbol{r_0}$ (diameter $\mathbf{d_0 = 2r_0}$);
- a shell-shaped interphase of external radius **a**, thickness $\mathbf{t = a - r_0}$, and uniform properties;
- a volume of matrix with size much greater than **a** and $\mathbf{r_0}$.

The properties required by the analysis can be computed by means of Molecular Dynamics (MD) simulations, as done in [24,25], which provide, as outputs, the radial extension of the interphase as well as its elastic properties averaged through the thickness. Alternatively, for a specific system, they could be fitted *a posteriori* on the basis of dedicated experimental results.

2.2.2. Application of the multiscale approach

The system at the macro-scale is constituted of a cracked nano-modified matrix (see Fig. 3). Under the hypothesis of plane strain conditions, with reference to the coordinate system shown in Fig. 3, the stress components at the crack tip can be divided into a hydrostatic part:

$$\sigma_h = \frac{\sigma_x + \sigma_y + \sigma_z}{3} = \frac{2(1+\nu_0)K_I}{3\sqrt{2\pi\rho}}\cos\frac{\phi}{2} \tag{2}$$

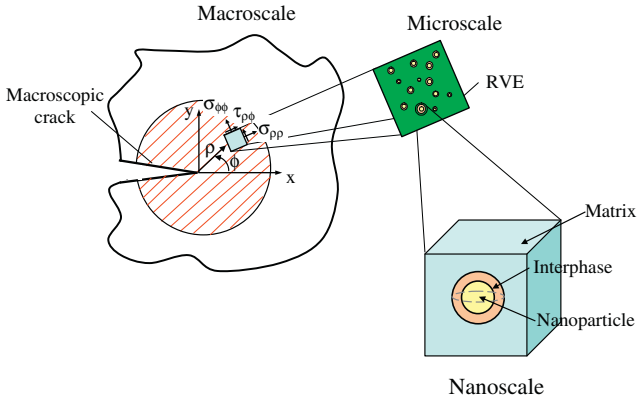

Fig. 3. Description of the multiscale system under analysis.

and a deviatoric one:

$$\begin{Bmatrix} s_{xx} \\ s_{yy} \\ s_{zz} \\ \tau_{xy} \end{Bmatrix} = \begin{Bmatrix} \sigma_{xx} - \sigma_h \\ \sigma_{yy} - \sigma_h \\ \sigma_{zz} - \sigma_h \\ \tau_{xy} \end{Bmatrix} = \frac{K_I}{\sqrt{2\pi\rho}} \times \begin{Bmatrix} \frac{1}{6}\cos\frac{\phi}{2}[2(1-2\nu_0) - 3Cos\,\phi + 3Cos\,2\phi] \\ \frac{1}{6}\cos\frac{\phi}{2}[2(1-2\nu_0) + 3Cos\,\phi - 3Cos\,2\phi] \\ \frac{2}{3}(2\nu_0 - 1)\cos\frac{\phi}{2} \\ \cos\frac{\phi}{2}\sin\frac{\phi}{2}\cos\frac{3\phi}{2} \end{Bmatrix} \tag{3}$$

where K_I and ν_0 are the Stress Intensity Factor of local stress fields and the Poisson's ratio of the nanocomposite, respectively. The stress field given by Eq. (3) can also be represented in terms of principal stresses; by doing so one obtains:

$$s = \begin{Bmatrix} s_{11} \\ s_{22} \\ s_{33} \end{Bmatrix} = \frac{K_I}{\sqrt{2\pi\rho}} \begin{Bmatrix} \frac{(1-2\nu_0)}{3}\cos\frac{\phi}{2} - \frac{1}{2}\sin\phi \\ \frac{(1-2\nu_0)}{3}\cos\frac{\phi}{2} + \frac{1}{2}\sin\phi \\ -\frac{2}{3}(1-2\nu_0)\cos\frac{\phi}{2} \end{Bmatrix} \tag{4}$$

The associated equivalent macroscopic von Mises stress is:

$$\sigma_{vM} = \frac{K_I}{\sqrt{4\pi\rho}}\cos\frac{\phi}{2}\sqrt{2(1-2\nu_0)^2 + 3(1-\cos\phi)} \tag{5}$$

Within a multiscale approach to the problem, in agreement with the concepts provided in Section 2.1, the deviatoric crack macroscale stress field s can be regarded as the average value of the microscale stresses over a Representative Volume Element (RVE). The bridge with the nanoscale can finally be established by means of the Mori–Tanaka approach (see Fig. 1).

Then, the maximum von Mises stress and the hydrostatic stress arising around the nanoparticle can be approximated by:

$$\sigma_{vM,n} = H_{vM}\sigma_{vM} = H_{vM}\frac{K_I}{\sqrt{4\pi\rho}}\cos\frac{\phi}{2}\sqrt{2(1-2\nu_0)^2 + 3(1-\cos\phi)} \tag{6}$$

$$\sigma_{h,n} = H_h\sigma_h = H_h\frac{2(1+\nu_0)K_I}{3\sqrt{2\pi\rho}}\cos\frac{\phi}{2} \tag{7}$$

where H_h is the hydrostatic part the of the global stress concentration tensor and, under the hypothesis of a rigid nanoparticle, can be determined as [9]:

$$H_h = \frac{\left(\frac{3K_a}{G_m} + 4\frac{G_a}{G_m}\right)\left(\frac{3(1-\nu_m)}{1+\nu_m}\right)}{\frac{3K_a}{G_m} + 4 - 4\cdot\left(1 - \frac{G_a}{G_m}\right)(r_0/a)^3} \tag{8}$$

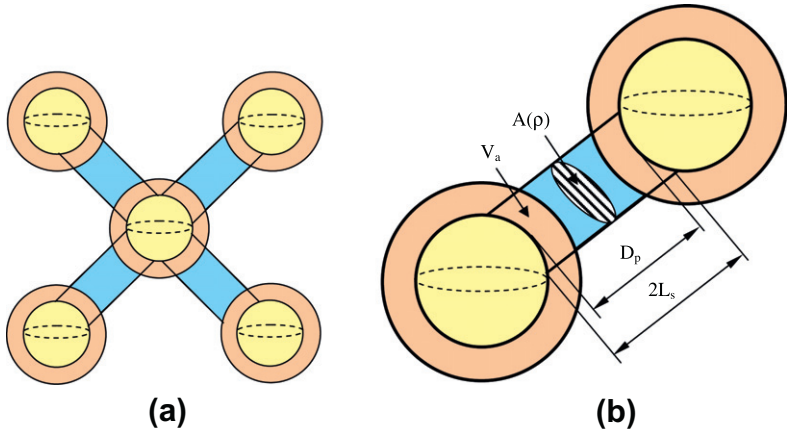

Fig. 4. Schematic representation of the four plastic shear bands departing from a nanoparticle (a). Relevant geometrical quantities used to describe the localised shear banding around nanoparticles (b).

Differently, H_{vM} is the deviatoric component of the global stress concentration tensor, and it is determined in closed form in Appendix A.

Whenever the stress field around a nanoparticle is high enough, it causes local shear yielding, with the formation of plastic shear bands. The region of material containing all the nanoparticles subjected to shear yielding is denoted as Shear Banding Region (SBR). According to [3–5,12], the shear bands are modelled as four plastic strips departing from the nanoparticle periphery (Fig. 4a). As we will argue better later, the size of these strips depends on the distance from the crack tip.

The extension of the SBR can be determined by applying the modified von Mises yielding criterion, which explicitly takes into account the level of the hydrostatic stress [26]:

$$\sigma_{vM,n} + \sqrt{3}\mu\sigma_{h,n} = \sigma_{Ya,c}\left(1 - \frac{\mu}{\sqrt{3}}\right)^2 \tag{9}$$

where $\sigma_{Ya,c}$ is the interphase yield stress under compression and μ is a dimensionless pressure coefficient. Substituting Eqs. (6) and (7) and solving by ρ:

$$\rho_{SB}(\phi) = \frac{1}{4\pi}\left[\frac{K_I}{\sigma_{Ya,c}(1-\mu/\sqrt{3})}\right]^2 \left[H_{vM}\sqrt{2(1-2\nu_0)^2 + 3(1-\cos\phi)} + \sqrt{8/3}\mu H_h(1+\nu_0)\right]^2 \cos^2\frac{\phi}{2} \tag{10}$$

Eq. (10) gives the region of the material subjected to shear banding (SBR). From Eq. (10) it is also evident that the actual value of ρ_{SB} strongly depends on ϕ. However, the use of an average value for the extension of the damage zone makes it representative of the overall damage behaviour over ϕ. Such an average value can be defined as:

$$\bar{\rho}_{SB} = \frac{1}{2\pi}\int_{-\pi}^{+\pi}\rho_{SB}(\phi)d\phi = \frac{1}{4\pi}\left[\frac{K_I}{\sigma_{Ya,c}(1-\mu/\sqrt{3})}\right]^2 I_{SB} \tag{11}$$

where:

$$I_{SB} = \frac{1}{2\pi}\int_{-\pi}^{+\pi}\left[H_{vM}\sqrt{2(1-2\nu_0)^2 + 3(1-\cos\phi)} + \sqrt{8/3}\mu H_h(1+\nu_0)\right]^2 \times \cos^2\frac{\phi}{2}d\phi \tag{12}$$

The analytical solution for I_{SB} is given in Appendix B.

Then, in the following we approximate the actual SBR with a circle, centred at the crack tip and having a radius equal to $\bar{\rho}_{SB}$. This is in agreement with [4,5,12].

Denoting with U_{SB} the energy produced at the nanoscale, according to the adopted multiscale system, the strain energy density in a RVE (microscale) can be calculated as:

$$u_{SB} = U_{SB} \times \frac{3f_{p0}}{4\pi r_0^3} \tag{13}$$

where f_{p0} is the volume fraction of nanoparticles. Finally, the fracture toughness enhancement due to shear band formation can be determined, according to [4,5,7,12,27,28] as:

$$\Delta G_{SB} = 2 \times \int_0^{\bar{\rho}_{SB}} u_{SB}d\rho \tag{14}$$

The problem of determining the overall fracture toughness enhancement is, in this way, reconverted into finding the energy produced at the nanoscale by shear banding.

3. Modelling of toughness improvements due to shear bands

In a recent work, analysing the transmission optical micrographs from the (non-propagating) crack-tip region of DN4PB test specimens, Hsieh et al. [4,5] demonstrated the tendency of the epoxy polymers to form localised plastic shear bands. In agreement with previous works [4,5,12], this phenomenon of localised damage can be modeled using a very simple network according to which the local stress concentration around each nanoparticle gives rise to four shear bands, departing from the nanoparticle surface. According to this schematic, the cross sectional area of the single shear band soundly scales with the diametrical cross sectional of the nanoparticle as:

$$A(\rho) = f(\rho)\pi r_0^2 \tag{15}$$

In this expression, $f(\rho)$, of which the values must fall within the range (0,1), is an appropriate function of the distance from the crack tip. A convenient form for $f(\rho)$ is the following power expression:

$$f(\rho) = 1 - \left(\frac{\rho}{\bar{\rho}_{SB}}\right)^{\alpha} \tag{16}$$

For the sake of simplicity, in this work we assume $\alpha = 0.5$, where the square root law has been chosen to agree with the square root singularity.

The length of the shear bands can then be estimated as:

$$L_s = r_0 + \frac{D_p}{2} - r_0\sqrt{1-f(\rho)} \tag{17}$$

where D_p is the interparticle distance. Under the hypothesis of a cubic array, which is likely to occur for low nanofiller volume fractions, D_p can be estimated as:

$$D_p = \left[\left(\frac{4\pi}{3f_{p0}}\right)^{\frac{1}{3}} - 2\right] r_0 \tag{18}$$

It is worth noting (see Fig. 4b) that in this paper it has been considered the presence of an interphase zone between the nanoparticle and the matrix, thought of a zone of matrix of altered chemistry. Then the shear band departing from the nanoparticle boundary develops partly in the interphase zone and partly in the un-altered matrix. It is then basic to estimate the volume fraction of the interphase and of the matrix which have encountered shear yielding.

With the aid of simple geometrical considerations, the total volume of the shear yielded material can be estimated by:

$$V_{tot} = \frac{3f_{p0}}{\pi r_0^3}\left[\pi f(\rho) r_0^2 L_s - \frac{\pi}{3}\left(L_s - \frac{D_p}{2}\right)^2\left(3r_0 - L_s + \frac{D_p}{2}\right)\right] \tag{19}$$

The interphase volume fraction per unit volume within the bands can be expressed, instead, by means of the following equation, for $D_p \geqslant 2t$:

$$\begin{aligned} V_a = \frac{3f_{p0}}{\pi r_0^3}\Bigg[&\pi f(\rho) r_0^2\left(r_0\sqrt{\left(\frac{a}{r_0}\right)^2 - f(\rho)} - r_0 + L_s - \frac{D_p}{2}\right) \\ &- \frac{\pi}{3}\left(L_s - \frac{D_p}{2}\right)^2\left(3r_0 - L_s + \frac{D_p}{2}\right) + \frac{\pi}{3} r_0^3\left(\frac{a}{r_0} - \sqrt{\left(\frac{a}{r_0}\right)^2 - f(\rho)}\right)^2 \\ &\times\left(2\frac{a}{r_0} + \sqrt{\left(\frac{a}{r_0}\right)^2 - f(\rho)}\right)\Bigg] \end{aligned} \tag{20}$$

Finally, the matrix fraction can be evaluated as:

$$V_m = \frac{3f_{p0}}{\pi r_0^3}\left[\pi f(\rho) r_0^2 L_s - \frac{\pi}{3}\left(L_s - \frac{D_p}{2}\right)^2\left(3r_0 - L_s + \frac{D_p}{2}\right)\right] - V_a \tag{21}$$

If we assume, for the sake of simplicity, that the matrix and the interphase yield according to a perfectly plastic law, we can disregard the elastic part of the stress–strain curve, and determine the strain energy density related to shear banding as:

$$u_{SB} = f(\rho)\tau_{ym} V_m \gamma_{fm} + f(\rho)\tau_{ya} V_a \gamma_{fa} = u_m + u_a \tag{22}$$

where τ_{ym} and τ_{ya} are the shear yielding stress of the matrix and of the interphase, while γ_{fm} and γ_{fa} are the shear fracture strain of the matrix and of the interphase, respectively.

Substituting Eq. (22) into Eq. (14) results in:

$$\begin{aligned} \Delta G_{SB} = &2\int_0^{\rho_{SB}} u_{SB} d\rho = \bar{\rho}_{SB} f_{p0}\tau_{ym}\gamma_{fm}\left\{\left(\frac{\pi}{6f_{p0}}\right)^{\frac{1}{3}} - \frac{52}{63}\frac{\tau_{ya}\gamma_{fa}}{\tau_{ym}\gamma_{fm}}\right. \\ &\left. - \left(1 - \frac{\tau_{ya}\gamma_{fa}}{\tau_{ym}\gamma_{fm}}\right)\left[\frac{32}{21}Q\left(\frac{1}{3} + \frac{\bar{a}^4}{5}\right) + \frac{\bar{a}^2}{315}(4S - 32\bar{a}^4 Z + 128\bar{a}^6 M)\right]\right\} \\ = &\bar{\rho}_{SB} f_{p0} \Gamma \end{aligned} \tag{23}$$

where:

$$\begin{aligned} \Gamma = &\tau_{ym}\gamma_{fm}\left\{\left(\frac{\pi}{6f_{p0}}\right)^{\frac{1}{3}} - \frac{52}{63}\frac{\tau_{ya}\gamma_{fa}}{\tau_{ym}\gamma_{fm}} - \left(1 - \frac{\tau_{ya}\gamma_{fa}}{\tau_{ym}\gamma_{fm}}\right)\right. \\ &\left. \times\left[\frac{32}{21}Q\left(\frac{1}{3} + \frac{\bar{a}^4}{5}\right) + \frac{\bar{a}^2}{315}(4S - 32\bar{a}^4 Z + 128\bar{a}^6 M)\right]\right\} \end{aligned} \tag{24a}$$

$$\bar{a} = \frac{a}{r_0} \quad Q = \sqrt{\bar{a}^2 - 1} \quad M = \bar{a} - Q \quad S = 105\bar{a} - 88Q$$
$$Z = 9\bar{a} - 7Q \tag{24b}$$

and $\bar{\rho}_{SB}$ is given by Eq. (11).

Further taking into consideration that:

$$G_I = K_I^2(1 - \nu_0^2)/E_0 \tag{25}$$

the fracture toughness improvement turns finally out to be:

$$\begin{aligned} \Delta G_{SB} &= G_{Ic} f_{p0} \times \left(\frac{I_{SB}}{4\pi\sigma_{ya}^2(1 - \mu\sqrt{3})^2}\frac{E_0}{1 - \nu_0^2} \times \Gamma\right) \\ &= f_{p0} \times \psi_{SB} \times G_{Ic} \end{aligned} \tag{26}$$

where ψ_{SB} quantifies the energy dissipation at the nanoscale by localised shear banding:

$$\psi_{SB} = \left(\frac{I_{SB}}{4\pi\sigma_{ya}^2(1 - \mu/\sqrt{3})^2}\frac{E_0}{1 - \nu_0^2} \times \Gamma\right) \tag{27}$$

Since, according to [7,12], the overall fracture toughness can be written as:

$$G_{Ic} = G_{Im} + \Delta G_{SB} \tag{28}$$

being G_{Im} the fracture toughness of the pure (unloaded) matrix, the fracture toughness improvement can also be written in the following normalised form:

$$\frac{\Delta G_{SB}}{G_{Im}} = \frac{f_{p0} \times \psi_{SB}}{1 - f_{p0} \times \psi_{SB}} \tag{29}$$

4. Results and discussion

In the present work, a general multi-scale approach has been proposed for the damage analysis at the nanoscale induced by shear banding around nanoparticles. It has been assumed that the nanofiller is uniformly dispersed and distributed within the volume, agglomeration being neglected at present. The effect of an interphase zone surrounding the nanoparticle, characterised by mechanical properties different from those of the matrix, is explicitly considered.

Plastic shear bands are thought of as created by the stress concentration around nanoparticles. The shear bands are modelled as four plastic strips departing from the nanoparticle periphery (see Fig. 4a and b) of which the size depend on the distance from the crack tip. The extension of the SBR, the region of material containing all the nanoparticles causing to shear yielding, has been determined in closed form by applying the modified von Mises yielding criterion. This zone is thought of as the active process zone.

The aim of this section is to clarify the range of applicability and to highlight, through examples, the most relevant features of the solution proposed in the previous sections.

The following properties have been adopted for the matrix, according to the suggestions in Refs. [4,5]: $\tau_{ym} = 61.3$ MPa, $\gamma_{fm} = 0.75$, $E_m = 2.96$ GPa, $\nu_m = 0.35$. Conversely, the properties of the interphase have been changed in order to analyse their contribution to the final solution.

The effect of the interphase zone on the total strain energy, u_{tot}, dissipated within the RVE, Eq. (22), is shown in Fig. 5. In the figure, the strain energy absorbed within the matrix, u_m, the interphase, u_a, and the total energy absorbed, u_{tot}, normalised to the maximum total strain energy, $u_{tot,max}$, are plotted as a function of the nanoparticle radius for given interphase thickness and ultimate properties. It is worth noting that, moving from micro to nanoparticles, the fraction of energy dissipated within the interphase, u_a, increases. Fig. 5 also shows, with reference to the case investigated,

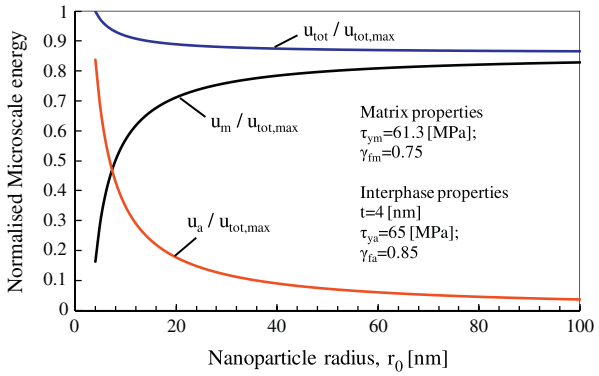

Fig. 5. Normalised microscale energy dissipated by shear banding within the matrix, u_m, and the interphase, u_a, as a function of the nanoparticle radius ($f(\rho)$ equal to 0.5).

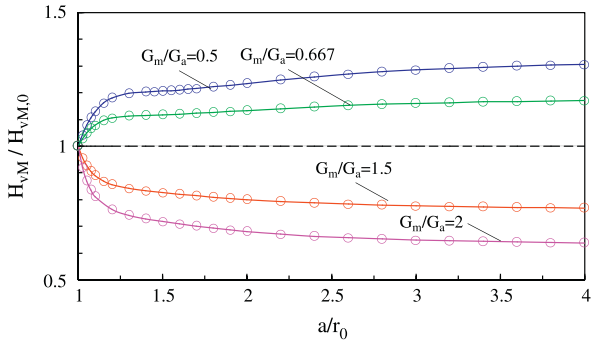

Fig. 6. Influence of the interphase properties on the von Mises stress concentration around nanoparticles, according to Eq. (A.21). $H_{vM,0}$ is the stress concentration disregarding the interphase.

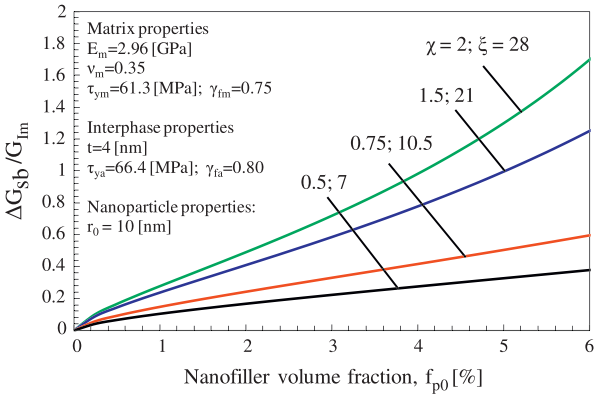

Fig. 7. Normalised fracture toughness increment due to shear banding as a function of the nanofiller volume fraction. Different interphase elastic properties ($\chi = G_a/G_m$; $\xi = 3K_a/G_m$).

the strong size dependency of the phenomenon, the contribution of the interphase becoming lower than 10% for nanoparticle diameters larger than 60 nm.

It is also worth noting, in addition, that the interphase elastic properties highly affects the stress concentration at the nanoparticle periphery. In Fig. 6, the normalised von Mises stress concentration factor, determined by accounting for the presence of the interphase, is plotted as a function of a/r_0, considering different

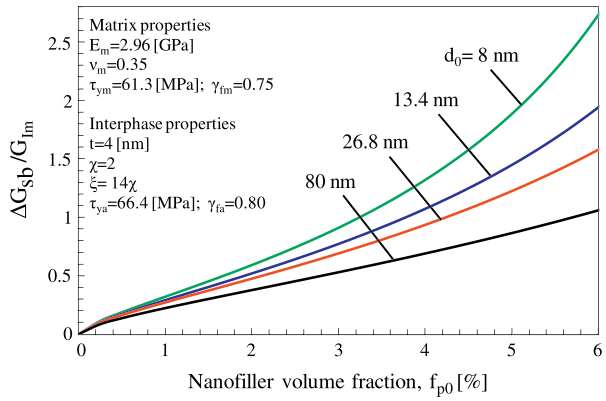

Fig. 8. Normalised fracture toughness increment as a function of the nanofiller volume fraction. Stiff interphase ($\chi = G_a/G_m = 2$; $\xi = 3K_a/G_m = 28$). Different nanoparticle diameters ($d_0 = 2r_0$).

interphase elastic properties. It can be seen that the stiffer the interphase, the higher H_{vM}, which reaches an almost asymptotic value for a/r_0 higher than 2. This leads to, ceteris paribus, a higher extension of the shear banding process zone, see Eqs. (11) and (12), and, in turn, in a much higher fracture toughness improvement, according to Eq. (26).

The analytical model developed in this work indicates that the fracture toughness improvements of nanoparticle reinforced polymers is mainly affected by two important parameters: the elastic properties of the interphase (related to the surface functionalisation of nanoparticles) and the nanofiller size. This is shown in Figs. 7–10.

In particular, Fig. 7 shows the fracture toughness increase due to shear banding as a function of the nanofiller volume content, for different elastic properties of the interphase. The model shows that the formation of local shear bands is a highly dissipative mechanism (causing a high fracture toughness improvement at low nanofiller content) and it is affected by the characteristics of the interphase. In this sense, the model agrees with the experimental evidence: as different functionalizers lead to different properties of the interphase, nanocomposite toughening may be strongly affected by surface treatments.

Differently, Figs. 8 and 9 show the influence of the particle size on the fracture toughness improvements, such an effect being different depending whether the interface is stiffer or softer than the matrix. In Fig. 8, the case of an interphase stiffer than the matrix is presented. The toughness increase becomes more than 200% and it is higher for smaller nanoparticles.

With reference to the case of a soft interphase, Fig. 9 shows that the increase is smaller with respect to the previous case and greater nanoparticle radii lead to higher fracture toughness.

To better clarify the size effect on the model, the toughness improvement is shown in Fig. 10 versus the nanoparticle radius for two different interphase properties and a volume fraction of 5%. For radii higher than 60 nm, the results for both the case of a soft interphase and of a stiff interphase lead to the same asymptotic value. Instead, for smaller particles, a stiff interphase gives far higher improvements than a soft one.

It is worth noting that as a basic assumption of the present work the nanofiller is supposed to be uniformly dispersed and distributed, neglecting the high tendency to agglomerate exhibited by nanoparticles beyond a certain value of the volume fraction. It is clear that this approximation confines the application of the model to low nanofiller volume fractions.

Eventually, it is important to remember that a correct prediction of the fracture toughness of nanoparticle filled polymers should include, besides the effect of the shear bands, the amount

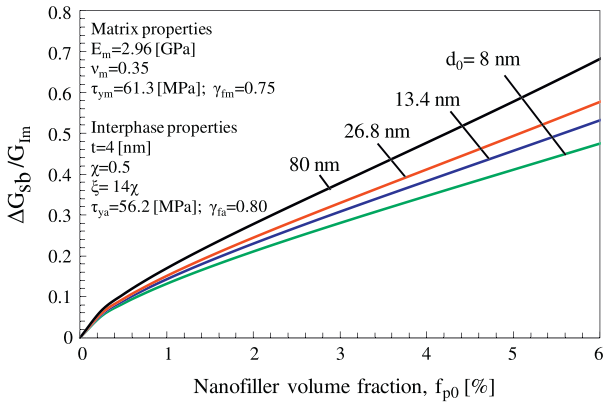

Fig. 9. Normalised fracture toughness increment as a function of the nanofiller volume fraction. Soft interphase ($\chi = G_a/G_m = 0.5$; $\xi = 3K_a/G_m = 7$). Different nanoparticle diameters ($d_0 = 2r_0$).

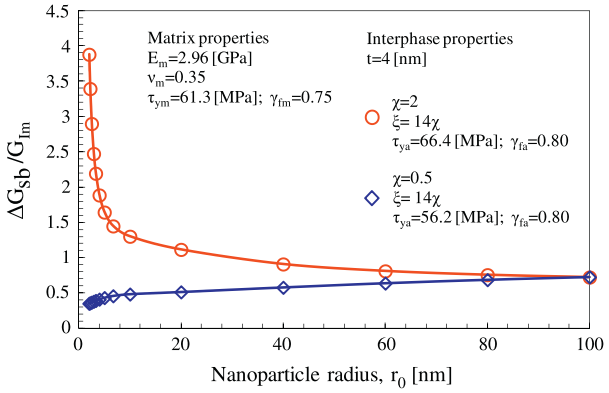

Fig. 10. Normalised fracture toughness increment as a function of the nanoparticle radius for a volume fraction, f_{p0}, of 5%.

Table 1
Comparison between the fracture toughness of an epoxy matrix filled with silica nanoparticles [5] and the theoretical predictions including the contribution due to shear bands only.

Silica volume fraction, f_{p0}	G_{IC} (experiments) (J/m^2)	G_{IC} (estimated) (J/m^2)
0	77	–
0.025	123	100.8
0.049	179	117.1
0.071	183	131.8

of energy dissipated by other mechanisms taking place at the nanoscale (like, for example, the plastic yielding of nanovoids [15]) which are not dealt with in the present work. Indeed, the assessments based solely on the multiscale model developed in this work inevitably lead to an underestimation of the fracture toughness for nanoparticle filled polymers. However, for the sake of completeness, Table 1 shows a comparison between the fracture toughness of an epoxy matrix filled with silica nanoparticles [5] and the theoretical predictions including the contribution due to shear bands only. As expected, the model underestimates the fracture toughness of polymer nanocomposites.

5. Conclusion

An analysis is provided for the toughening of nanoparticle filled polymers caused by the emergence of localised plastic shear bands, initiated by the stress concentrations around nanoparticles. The model stems from the quantification of the energy absorbed at the nanoscale and accounts for the emergence of an interphase, created by the inter- and supra-molecular interactions arising at the nanoscale, with mechanical properties different from those of the matrix. It is proved that the interphase elastic properties highly affect the stress rising around particles, causing lower or higher energy dissipation at the nanoscale. Moreover it is proved that the particle size effects may be different depending on the elastic properties of the interphase.

Acknowledgment

The financial support to the activity by Veneto Nanotech, the Italian Cluster of Nanotechnology (Padova, Italy), is greatly acknowledged.

Appendix A. Determination of coefficient H_{vM}

Let consider the problem shown in Fig. A1a. The deviatoric part of the interphase stress components around the nanoparticle, at $r = r_0$, can be written as [29]:

$$\begin{aligned}\sigma_{rrd,a} &= \sigma(\bar{A}_a \cos^2\theta_2 + \bar{B}_a)\\ \sigma_{\theta\theta d,a} &= \sigma(\bar{C}_a \cos^2\theta_2 + \bar{D}_a)\\ \sigma_{\phi\phi d,a} &= \sigma(\bar{E}_a \cos^2\theta_2 + \bar{F}_a)\\ \tau_{r\theta,a} &= \sigma\bar{H}_a \cos\theta_2 \sin\theta_2\end{aligned} \tag{A.1}$$

where:

$$\bar{A}_a = \frac{3G_a}{\alpha+\beta+\chi+\delta}\left[-\frac{\omega}{14} - \xi\frac{9\lambda_a+10G_a}{6\lambda_a} + \eta + 6\kappa\right] \tag{A.2}$$

$$\bar{B}_a = -\frac{G_a}{\alpha+\beta+\chi+\delta}\left[-\frac{\omega}{14} - \xi\frac{9\lambda_a+10G_a}{6\lambda_a} + \eta + 6\kappa\right] \tag{A.3}$$

$$\bar{C}_a = \frac{G_a}{\alpha+\beta+\chi+\delta}\left[-\omega\frac{5\lambda_a+4G_a}{2\lambda_a} + \xi\frac{G_a}{2\lambda_a} - 3\eta - \frac{21}{2}\kappa\right] \tag{A.4}$$

$$\bar{D}_a = \frac{G_a}{\alpha+\beta+\chi+\delta}\left[\omega\frac{15\lambda_a+14G_a}{14\lambda_a} + \xi\frac{G_a}{6\lambda_a} + 2\eta + \frac{9}{2}\kappa\right] \tag{A.5}$$

$$\bar{E}_a = \frac{G_a}{\alpha+\beta+\chi+\delta}\left[-\omega\frac{25\lambda_a+14G_a}{14\lambda_a} + \frac{3}{2}\xi\frac{G_a}{\lambda_a} - \frac{15}{2}\kappa\right] \tag{A.6}$$

$$\bar{F}_a = -\frac{G_a}{\alpha+\beta+\chi+\delta}\left[-\frac{5}{14}\omega + \frac{5}{6}\xi\frac{G_a}{\lambda_a} + \eta - \frac{3}{2}\kappa\right] \tag{A.7}$$

$$\bar{H}_a = -\frac{G_a}{\alpha+\beta+\chi+\delta}\left[\omega\frac{8\lambda_a+7G_a}{7\lambda_a} + \xi\frac{3\lambda_a+2G_a}{2\lambda_a} + 3\eta - 12\kappa\right] \tag{A.8}$$

Auxiliary parameters are defined as [29]:

$$\begin{aligned}\alpha = {} & 28G_a^4\cdot(8G_m+3\lambda_m)(28+50\bar{a}^3-36\bar{a}^5+25\bar{a}^7+8\bar{a}^{10})\\ & + 12G_m^2\cdot\lambda_a^2\cdot(14G_m+9\lambda_m)(\bar{a}-1)^4\cdot(4+16\bar{a}+40\bar{a}^2\\ & + 55\bar{a}^3+40\bar{a}^4+16\bar{a}^5+4\bar{a}^6)\end{aligned} \tag{A.9}$$

$$\begin{aligned}\beta = {} & 4G_a^3\{2G_m[7G_m(-224-25\bar{a}^3+18\bar{a}^5+75\bar{a}^7+156\bar{a}^{10})\\ & +4\lambda_a\cdot(182+400\bar{a}^3-504\bar{a}^5+350\bar{a}^7+97\bar{a}^{10})] + 3\lambda_m\\ & \cdot[7G_m(-76+25\bar{a}^3-18\bar{a}^5+25\bar{a}^7+44\bar{a}^{10}) + \lambda_a(182+400\bar{a}^3\\ & -504\bar{a}^5+350\bar{a}^7+97\bar{a}^{10})]\}\end{aligned} \tag{A.10}$$

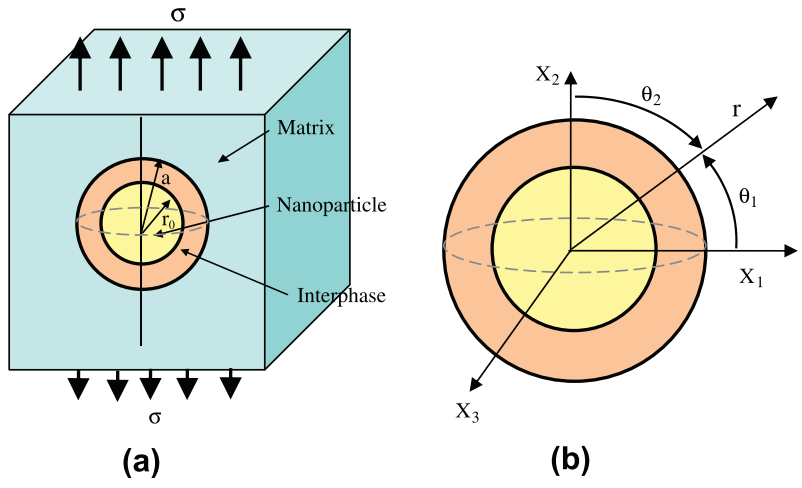

Fig. A1. Spherical inclusion embedded in a shell-shaped interphased zone under unidirectional load (a). Polar coordinate system used to describe the stress field around the nanoparticle (b).

$$\chi = G_a G_m \lambda_a \Big\{ 112 G_m^2 (37 - 100\bar{a}^3 + 126\bar{a}^5 - 100\bar{a}^7 + 37\bar{a}^{10}) + 9\lambda_a \lambda_m \cdot (-96 + 100\bar{a}^3 - 168\bar{a}^5 + 75\bar{a}^7 + 89\bar{a}^{10}) + 6 \cdot G_m [\lambda_a (-304 - 100\bar{a}^3 + 168\bar{a}^5 - 25\bar{a}^7 + 261\bar{a}^{10}) + 12\lambda_m (37 - 100\bar{a}^3 + 126\bar{a}^5 - 100\bar{a}^7 + 37\bar{a}^{10})] \Big\} \quad (A.11)$$

$$\delta = G_a^2 \Big\{ 392 G_m^3 (16 - 25\bar{a}^3 + 18\bar{a}^5 - 25\bar{a}^7 + 16\bar{a}^{10}) + 9\lambda_a^2 \lambda_m \cdot (48 + 200\bar{a}^3 - 336\bar{a}^5 + 225\bar{a}^7 + 38\bar{a}^{10}) + 4 \cdot G_m^2 [\lambda_a (-2492 - 400\bar{a}^3 + 504\bar{a}^5 + 525\bar{a}^7 + 1863\bar{a}^{10}) + 63\lambda_m (16 - 25\bar{a}^3 + 18\bar{a}^5 - 25\bar{a}^7 + 16\bar{a}^{10})] + 6 G_m \lambda_a [4\lambda_a (48 + 200\bar{a}^3 - 336\bar{a}^5 + 225\bar{a}^7 + 38\bar{a}^{10}) + \lambda_m (-808 + 400\bar{a}^3 - 504\bar{a}^5 + 325\bar{a}^7 + 587\bar{a}^{10})] \Big\} \quad (A.12)$$

$$\xi = -75\bar{a}^3 \lambda_a (2G_m + \lambda_m) \{ 14 G_a [G_a \cdot (4 + \bar{a}^7) + 4 G_m (\bar{a}^7 - 1)] + \lambda_a \cdot [G_a (16 + 19\bar{a}^7) + 16 \cdot G_m (\bar{a}^7 - 1)] \} \quad (A.13)$$

$$\omega = 6300\bar{a}^3 (\bar{a}^2 - 1)\, \lambda_a (G_a - G_m)(G_a + \lambda_a)(2G_m + \lambda_m) \quad (A.14)$$

$$\eta = 5\bar{a}^3 (2G_m + \lambda_m) \Big\{ 28 G_a^2 [G_a \cdot (25 - 9\bar{a}^2 + 4\bar{a}^7) + G_m (-25 + 9\bar{a}^2 + 16\bar{a}^7)] + 2\lambda_a G_a \cdot [G_a (400 - 252\bar{a}^2 + 97\bar{a}^7) + 4 \cdot G_m (-100 + 63\bar{a}^2 + 37\bar{a}^7)] + 3\lambda_a^2 \cdot [G_a \cdot (100 - 84\bar{a}^2 + 19\bar{a}^7) + 4 G_m \cdot (-25 + 21\bar{a}^2 + 4\bar{a}^7)] \Big\} \quad (A.15)$$

$$\kappa = -15\bar{a}^5 (2G_m + \lambda_m)(G_a + \lambda_a) \{ 14 G_a \cdot [G_a (4 + \bar{a}^5) + 4 G_m (\bar{a}^5 - 1)] + \lambda_a \cdot [G_a (16 + 19\bar{a}^5) + 16 G_m (\bar{a}^5 - 1)] \} \quad (A.16)$$

where $\bar{a} = a/r_0$.

This analytical framework can be used to calculate analytically coefficient H_{vM}. According to the analysis carried out in Section 2.2, the macroscale deviatoric stress field and the macroscale equivalent von Mises stress turn out to be:

$$s = \begin{Bmatrix} s_{11} \\ s_{22} \\ s_{33} \end{Bmatrix} = \frac{K_I}{\sqrt{2\pi\rho}} \begin{Bmatrix} \frac{(1-2\nu_0)}{3} \cos\frac{\phi}{2} - \frac{1}{2}\sin\phi \\ \frac{(1-2\nu_0)}{3} \cos\frac{\phi}{2} + \frac{1}{2}\sin\phi \\ -\frac{2}{3}(1-2\nu_0)\cos\frac{\phi}{2} \end{Bmatrix}$$

$$\sigma_{vM} = \frac{K_I}{\sqrt{4\pi\rho}} \cos\frac{\phi}{2} \sqrt{2\,(1-2\nu_0)^2 + 3(1-\cos\phi)} \quad (A.17)$$

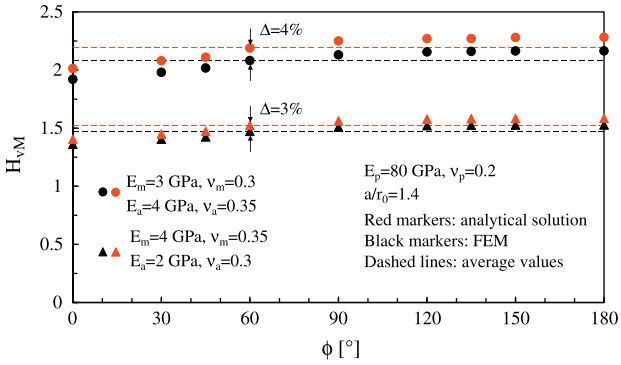

Fig. A2. Distribution of H_{vM} in the range $\phi \in [0, 180]$ for an interphase stiffer or softer than the matrix.

Coefficient H_{vM} represents the maximum von Mises stress at the periphery of the nanoparticle (nanoscale stress) when the system shown in Fig. A1a is loaded by a stress tensor constituted by a combination of stresses s_{11}, s_{22}, s_{33}, as given by Eq. (A.17).

In particular we suppose that the directions (X_1, X_2, X_3) of the Cartesian coordinate system shown in Fig. A1b coincides with the direction of applied stresses s_{11}, s_{22}, s_{33}.

It is evident that the value of coefficient H_{vM} depends on the angle ϕ. However the variation of H_{vM} in the range $\phi \in [0, 180]$ is very limited, and the value evaluated at $\phi = 60°$ can be regarded as representative of the average value (as an example see Fig. A2).

At $\phi = 60°$, the stress components s_{ij} can also be re-written in the following normalised form:

$$\begin{Bmatrix} \bar{s}_1 \\ \bar{s}_2 \\ \bar{s}_3 \end{Bmatrix} = \frac{1}{\sigma_{vM}} \begin{Bmatrix} s_{11} \\ s_{22} \\ s_{33} \end{Bmatrix} \quad (A.18)$$

When $\phi = 60°$, the maximum von Mises stress arising in the interphase at $r = r_0$ lays in the plane $X_3 = 0$. Accordingly:

$$\theta_2 = \text{Arc tan}\left(\frac{X_3}{X_1}\right) \quad \theta_1 = -\text{Arc tan}\left(\frac{X_3}{X_1}\right) = \theta_2 - \frac{\pi}{2} \quad \theta_3 = \frac{\pi}{2} \quad (A.19)$$

Then, by making use of Eq. (A.1) and using the superposition principle, the stress components in the interphase when $r = r_0$ can calculated as:

Table B1
Parameter K, E, j, k and p for some values of the Poisson's ratio.

v_0	K	E	j	k	p
0.05	2.2295	1.18691	9.23628	18.5339	9.80177
0.1	2.31597	1.16188	10.1369	18.1987	8.73363
0.15	2.41961	1.1363	11.0794	17.8071	7.79115
0.2	2.54568	1.11057	12.0637	17.3769	6.97434
0.25	2.70218	1.08526	13.09	16.9309	6.28319
0.3	2.90228	1.06109	14.1581	16.4986	5.7177
0.35	3.17028	1.03899	15.2681	16.1186	5.27788
0.4	3.56011	1.02016	16.4201	15.8447	4.96372
0.45	4.24255	1.00622	17.6139	15.7559	4.77522

$$\begin{aligned}
&\bar{\sigma}_{\mathrm{rrd,a}} = \overline{A}_{\mathrm{a}}(\bar{s}_1\cos^2\theta_1 + \bar{s}_2\cos^2\theta_2) + \overline{B}_{\mathrm{a}}(\bar{s}_1+\bar{s}_2+\bar{s}_3) = \overline{A}_{\mathrm{a}}(\bar{s}_1\cos^2\theta_1 + \bar{s}_2\cos^2\theta_2)\\
&\bar{\sigma}_{\theta\theta\mathrm{d,a}} = \overline{C}_{\mathrm{a}}(\bar{s}_1\cos^2\theta_1 + \bar{s}_2\cos^2\theta_2) + \overline{D}_{\mathrm{a}}(\bar{s}_1+\bar{s}_2+\bar{s}_3) = \overline{C}_{\mathrm{a}}(\bar{s}_1\cos^2\theta_1 + \bar{s}_2\cos^2\theta_2)\\
&\bar{\sigma}_{\phi\phi\mathrm{d,a}} = \overline{E}_{\mathrm{a}}(\bar{s}_1\cos^2\theta_1 + \bar{s}_2\cos^2\theta_2) + \overline{F}_9 m(\bar{s}_1+\bar{s}_2+\bar{s}_3) = \overline{E}_{\mathrm{a}}(\bar{s}_1\cos^2\theta_1 + \bar{s}_2\cos^2\theta_2)\\
&\bar{\tau}_{\mathrm{r}\theta,\mathrm{a}} = \overline{H}_{\mathrm{a}}(\bar{s}_1\cos\theta_1\sin\theta_1 + \bar{s}_2\cos\theta_2\sin\theta_2)
\end{aligned} \tag{A.20}$$

the latter substitution being valid because $\bar{s}_1+\bar{s}_2+\bar{s}_3 = 0$.

Coefficient H_{vM} can be determined as the maximum value of von Mises stress at the periphery of the nanoparticle, $\bar{\sigma}_{\mathrm{vM}}$, over the range $0 \leqslant \theta_2 \leqslant \pi/2$:

$$H_{\mathrm{vM}} = \max\{\bar{\sigma}_{\mathrm{vM}}\} \tag{A.21}$$

where:

$$\bar{\sigma}_{\mathrm{vM}} = \sqrt{\frac{(\bar{\sigma}_{\mathrm{rrd,a}}-\bar{\sigma}_{\theta\theta\mathrm{d,a}})^2 + (\bar{\sigma}_{\theta\theta\mathrm{d,a}}-\bar{\sigma}_{\phi\phi\mathrm{d,a}})^2 + (\bar{\sigma}_{\phi\phi\mathrm{d,a}}-\bar{\sigma}_{\mathrm{rrd,a}})^2 + 6\bar{\tau}^2_{\mathrm{r}\theta,\mathrm{a}}}{2}} \tag{A.22}$$

Appendix B. Closed form solution for integral I_{SB}

$$\begin{aligned}
I_{\mathrm{SB}} &= \frac{1}{2\pi}\int_{-\pi}^{+\pi}[H_{\mathrm{vM}}\sqrt{2(1-2v_0)^2+3(1-\cos\phi)}\\
&\quad + \sqrt{8/3}\mu H_{\mathrm{h}}(1+v_0)]^2\cos^2\frac{\phi}{2}d\phi\\
&= \frac{1}{2\pi}(pH_{\mathrm{vM}}^2 + k\mu H_{\mathrm{h}}H_{\mathrm{vM}} + j\mu^2H_{\mathrm{h}}^2)
\end{aligned} \tag{B.1}$$

where:

$$j = \frac{8}{3}\pi(1+v_0)^2 \tag{B.2}$$

$$\begin{aligned}
k = \frac{64}{27}\sqrt{3}\sqrt{1-v_0(1-v_0)}[2E(1+3v_0-2v_0^3) + K(1-3v_0\\
+ 4v_0^3)]
\end{aligned} \tag{B.3}$$

$$p = \frac{\pi}{2}(7-16v_0+16v_0^2) \tag{B.4}$$

$$K = \mathrm{Elliptic}K\left(\frac{3}{4-4v_0+4v_0^2}\right) \tag{B.5}$$

$$E = \mathrm{Elliptic}E\left(\frac{3}{4-4v_0+4v_0^2}\right) \tag{B.6}$$

being EllipticK and EllipticE the first and the second complete Elliptic integrals, respectively. Parameter K, E, j, k and p are listed in Table B1 for some values of the Poisson's ratio.

References

[1] Wetzel B, Rosso P, Haupert F, Friedrich K. Epoxy nanocomposites – fracture and toughening mechanisms. Eng Fract Mech 2006;73:2375–98.
[2] Zhao S, Schadler LS, Duncan R, Hillborg H, Auletta T. Mechanisms leading to improved mechanical performance in nanoscale alumina filled epoxy. Compos Sci Technol 2008;68:2965–75.
[3] Johnsen BB, Kinloch AJ, Mohammaed RD, Taylor AC, Sprenger S. Toughening mechanisms of nanoparticle-modified epoxy polymers. Polymer 2007;48:530–41.
[4] Hsieh TH, Kinloch AJ, Masania K, Taylor AC, Sprenger S. The mechanisms and mechanics of the toughening of epoxy polymers modified with silica nanoparticles. Polymer 2010;51:6284–94.
[5] Hsieh TH, Kinloch AJ, Masania K, Sohn Lee J, Taylor AC, Sprenger S. The toughness of epoxy polymers and fibre composites modified with rubber microparticles and silica nanoparticles. J Mater Sci 2010;45:1193–210.
[6] Quaresimin M, Salviato M, Zappalorto M. Strategies for the assessment of nanocomposite mechanical properties. Compos Part B – Eng 2012;43:2290–7.
[7] Lauke B. On the effect of particle size on fracture toughness of polymer composites. Compos Sci Technol 2008;68:3365–72.
[8] Chen JK, Huang ZP, Zhu J. Size effect of particles on the damage dissipation in nanocomposites. Compos Sci Technol 2007;14:2990–6.
[9] Zappalorto M, Salviato M, Quaresimin M. Influence of the interphase zone on the nanoparticle debonding stress. Compos Sci Technol 2011;72:49–55.
[10] Salviato M, Zappalorto M, Quaresimin M. The effect of surface stresses on the critical debonding stress around nanoparticles. Int J Fract 2011;172:97–103.
[11] Williams JG. Particle toughening of polymers by plastic void growth. Compos Sci Technol 2010;70:885–91.
[12] Huang Y, Kinloch AJ. Modelling of the toughening mechanisms in rubber-modified epoxy polymers. Part II a quantitative description of the microstructure-fracture property relationships. J Mater Sci 1992;27:2763–9.
[13] Zappalorto M, Salviato M, Quaresimin M. Assessment of debonding-induced toughening in nanocomposites. Procedia Eng 2011;10:2973–8.
[14] Salviato M, Zappalorto M, Quaresimin M. Plastic yielding around nanovoids. Procedia Eng 2011;10:3316–21.
[15] Zappalorto M, Salviato M, Quaresimin M. A multiscale model to describe nanocomposite fracture toughness enhancement by the plastic yielding of nanovoids. Compos Sci Technol 2012;72:1683–91.
[16] Timoshenko SP, Goodier JN. Theory of elasticity. 3rd ed. New York: McGraw-Hill; 1970.
[17] Bishop JFW, Hill RA. Theory of the plastic distortion of a polycrystalline aggregate under combined stresses. Philos Mag Series 7 1951;42:414–27.
[18] Hutchinson JW. Plastic stress–strain relation of F.C.C polycrystalline metals hardening according to Taylor's rule. J Mech Phys Solids 1964;12:11–24.
[19] Gurson AL. Continuum theory of ductile rupture by void nucleation and growth: Part I – yield criteria and flow rules for porous ductile media. J Eng Mater Technol 1977;99:2–15.
[20] Ajayan PM, Schadler LS, Braun PV. Nanocomposite science and technology. Wiley-VCH; 2003. ISBN 3527303596.
[21] Wichmann MHG, Cascione M, Fiedler B, Quaresimin M, Schulte K. Influence of surface treatment on mechanical behaviour of fumed silica/epoxy resin nanocomposites. Compos Interf 2006;13:699–715.
[22] Tian L, Rajapakse RKND. Elastic field of an isotropic matrix with a nanoscale elliptical inhomogeneity. Int J Solids Struct 2007;44:7988–8005.
[23] Sevostianov I, Kachanov M. Effect of interphase layers on the overall elastic and conductive properties of matrix composites. Applications to nanosize inclusion. Int J Solids Struct 2007;44:1304–15.
[24] Odegard GM, Clancy TC, Gates TS. Modeling of mechanical properties of nanoparticle/polymer composites. Polymer 2005;46:553–62.
[25] Yu S, Yang S, Cho M. Multi-scale modeling of cross-linked epoxy nanocomposites. Polymer 2009;50:945–52.
[26] Crist B. Yield processes in glassy polymers. In: Haward RN, Young RJ, editors. The physics of glassy polymers. Chapman & Hall; 1997.
[27] Freund LB, Hutchinson JW. High-strain-rate crack growth in rate dependent plastic solids. J Mech Phys Solids 1985;33:169–91.
[28] Evans AG, Williams S, Beaumont PWR. On the toughness of particulate filled polymers. J Mater Sci 1985;20:3668–74.
[29] Zappalorto M, Salviato M, Quaresimin M. Stress distributions around rigid nanoparticles. Int J Fract 2012;176:105–12.